Pharmaceutical Sciences 2026;32(4):566-579
doi:10.34172/ps.43968
https://ps.tbzmed.ac.ir

Original Article

Ergostane and Gorgastane Sterols Isolated from Soft Coral: *Sarcophyton tenuispiculatum* Thomson & Dean. with their Antibacterial, Anti-Biofilm, and Anti-Efflux Pump Activity Against Colistin-Resistant *acinetobacter Baumannii* Bacteria

Samin Mousavi,[1] Afsaneh Yegdaneh,[1*] Arezoo Mirzaei,[2] Hajar Sirous,[3] Mohammad Bagher Majnooni,[4] Melika Nazemi,[5] Mustafa Ghanadian[6*]

[1]Department of Pharmacognosy, School of Pharmacy and Pharmaceutical Sciences, Isfahan University of Medical Sciences, Isfahan, Iran
[2]Department of Bacteriology and Virology, Faculty of Medicine, Isfahan University of Medical Science, Isfahan, Iran
[3]Department of Bioinformatics, Bioinformatics Research Center, School of Pharmacy and Pharmaceutical Sciences, Isfahan University of Medical Sciences, Isfahan, Iran
[4]Pharmaceutical Sciences Research Center, Health Institute, Kermanshah University of Medical Sciences, Kermanshah, Iran
[5]Persian Gulf and Oman Sea Ecological Research, Agricultural Research, Education and Extension Organization, Iranian Fisheries Research Institute, Bandar Abbas, Iran
[6]Department of Phytochemistry, Isfahan Pharmaceutical Sciences Research Center, School of Pharmacy, Isfahan University of Medical Sciences, Isfahan, Iran

ARTICLE INFO

Article History:
Received: April 2, 2026
Revised: May 11, 2026
Accepted: June 8, 2026
ePublished: August 3, 2026

Keywords:
Soft Coral, *Sarcophyton tenuispiculatum*, Antibacterial Activity, Efflux Pump Inhibition, *Acinetobacter baumannii*

Abstract

Introduction: Soft corals are increasingly recognized for their antimicrobial potential. *Acinetobacter baumannii*, an opportunistic pathogen linked to pneumonia and urinary tract infections, often shows resistance to conventional therapies, including colistin. This resistance highlights the urgent need for novel agents with antibacterial and anti-biofilm properties. This study investigated the phytochemical composition and biological activities of steroids isolated from *Sarcophyton tenuispiculatum*, focusing on antibacterial, anti-biofilm, and efflux pump inhibitory effects against colistin-resistant *A. baumannii*. Soft coral specimens were collected from Larak Island, Iran, and subjected to phytochemical and biological evaluation, integrating experimental assays with molecular docking and ADMET analyses.

Methods: Bioactive metabolites were isolated by solvent partitioning, chromatography, and HPLC. Structures were characterized using NMR and GC-MS. Antibacterial, antibiofilm, and efflux pump inhibitory activities were assessed by MIC, diffusion, crystal violet, cartwheel, and qRT-PCR assays. Docking studies examined MexB binding, while ADMET predictions evaluated pharmacokinetics.

Results: Four steroids were identified: gorgosta-5-en-3β-ol(**1**), ergosta-5-en-3β-ol(**2**), ergosterol peroxide (**3**), and 5,8-epidioxy-ergosta-6-en-3-ol(**4**). Compounds **1**–**3** reduced biofilm formation (79%, 78%, 62%). Compound **1** showed strong efflux pump inhibition (MIC 500 µg/mL, $P<0.001$) and, with compound **2**, downregulated MexB gene expression. Docking revealed high binding affinities for compounds **1** and **2**, comparable to the co-crystallized ligand. ADMET analysis indicated favorable pharmacokinetics for compounds **1** and **2**, while compounds 3 and 4 showed mutagenic risks.

Conclusion: Steroids **1**–**3** displayed antibacterial and anti-biofilm activity against colistin-resistant *A. baumannii*. Compound **1** demonstrated the most promising profile, combining efflux pump inhibition, gene downregulation, and favorable pharmacokinetics, supporting its potential as a lead candidate for drug development.

Introduction

Marine organisms, such as soft corals, produce specialized secondary metabolites that protect them from harsh environmental conditions. Many species of these organisms inhabit the South China Sea. Members of the genus *Sarcophyton* (family Alcyoniidae) are known to produce secondary metabolites with anticancer, antimicrobial, and antifungal properties. [1]

These compounds display considerable structural diversity due to variations in their side chains, degrees of oxygenation, and rearrangements within their tetracyclic nuclei. The sterols found in soft corals are primarily derived

***Corresponding Author:** Mustafa Ghanadian, Email: ghannadian@gmail.com; Afsaneh Yegdaneh, Email: yekdaneh@pharm.mui.ac.ir

© 2026 The Author(s). This is an open access article and applies the Creative Commons Attribution Non-Commercial License (http://creativecommons.org/licenses/by-nc/4.0/). Non-commercial uses of the work are permitted, provided the original work is properly cited.

from cholestanes (27 carbon atoms), ergostanes (28 carbon atoms), 23,24-dimethylcholestanes (29 carbon atoms), and gorgostanes (30 carbon atoms). [2] Previous phytochemical and biological analysis of *Sarcophyton tenuispiculatum* has led to the identification of one hydroquinone derivative and several cembrane diterpenes. Pharmacological assays revealed that one autoxidized cembrane diterpene, (+)-7α,8β-dihydroxydeepoxysarcophine, inhibited IL-1β production in lipopolysaccharide (LPS)-stimulated macrophage cells. Additionally, the hydroquinone meroterpenoid demonstrated cytotoxicity against the MCF-7 and MDA-MB-231 cell lines. With the exception of one cembranoid (sarcotenusenes A), the others did not exhibit significant cytotoxic activity. [3]

Acinetobacter baumannii, a Gram-negative coccobacillus, is a significant opportunistic pathogen responsible for 2-10% of Gram-negative hospital-acquired infections. [4] According to the Infectious Diseases Society of America, *A. baumannii* is among the six most multidrug-resistant microorganisms in hospitals worldwide. [5] It is associated with a wide range of serious nosocomial infections, including ventilator-associated pneumonia (VAP), urinary tract infections, and bacteraemia in immunocompromised patients, leading to increased mortality and morbidity. [6]

In recent years, *A. baumannii* has emerged as an important cause of hospital-acquired infections because it can persist for long periods on nutrient-poor surfaces. [7] This persistence is attributed to its capacity to form biofilms, hydrated exopolysaccharide matrices that retain moisture and protect the bacteria from desiccation. These biofilms not only shield bacteria from environmental stress but also enhance survival and antibiotic resistance. In addition, efflux pumps such as MexB, as part of systems like MexAB-OprM, contribute to multidrug resistance. [8] Although certain antibiotics, such as colistin, have demonstrated efficacy against MDR *A. baumannii* in laboratory settings, their clinical use is limited due to severe side effects, including nephrotoxicity, kidney damage, neurotoxicity, and respiratory depression. [9] Moreover, colistin resistance, although still below 10% globally, is increasing in the Mediterranean, Southeast Asia, and parts of Africa, mainly due to biofilm formation and efflux pump activation. [10]

The novelty of this study lies in identifying the potential of *Sarcophyton*-derived steroids to inhibit biofilm formation and act as MexB efflux pump inhibitors in colistin-resistant *A. baumannii*. Accordingly, this study aims to isolate steroid compounds from the nonpolar fraction of *Sarcophyton tenuispiculatum* and evaluate their antibacterial, anti-biofilm, and anti-efflux pump activities against colistin-resistant *A. baumannii*, with particular focus on the inhibition of MexB gene expression and biofilm formation.

Materials and Methods

General experiments and procedures

Nuclear magnetic resonance (NMR) data were obtained using a Bruker 400 Ascend spectrometer operating at 400.13 MHz for proton nuclei and 100.62 MHz for carbon nuclei. Column chromatography was conducted on silica gel, while gel filtration chromatography utilized Sephadex LH-20 (Sigma-Aldrich). High-performance liquid chromatography (HPLC) was performed in isocratic mode on a preparative YMC-Silica column (20 × 25 cm) using a closed-loop recycling separation system.

Soft coral collection

Samples of *S. tenuispiculatum* were collected from the coast of Larak Island, Iran, during September and October of 2022 at a depth of 12 meters. The specimens were preserved at −20 °C until further use. Dr. Melika Nazemi, a specialist in marine taxonomy, performed taxonomic identification. A voucher specimen (PGOSERI.CNI.SAR.TEN.010) was deposited at the Department of Marine Biotechnology and Resources, Persian Gulf and Oman Sea Ecology Research Institute.

Extraction and isolation

Sample preparation was carried out using frozen coral specimens with a total wet weight of 17 kg. To inactivate the enzymes in the coral, the samples were placed in a beaker containing a 3% formaldehyde solution in an ice bath, with added salt, and then sonicated for a short duration (10 minutes). The corals were then rapidly squeezed to remove excess water, thereby preventing autooxidation and the activation of hydrolytic enzymes. The material was chopped into small pieces with gardening scissors, and 2.34 kg of it was subsequently dried overnight at room temperature (20–25 °C) in the laboratory. It was finely powdered for a uniform extraction. The powder was evenly distributed in the percolator and loosely packed to allow percolation. For extraction, approximately 35 liters of solvent (15 mL per gram of material) were used at a slow flow rate of about 7 mL/min (equivalent to three drops per second) at room temperature (20-25 °C). The extraction was performed in three cycles, each lasting approximately 24 hours, and continued until the extract became colorless. The *S. tenuispiculatum* (STE) extract was filtered and then evaporated in a rotary evaporator under vacuum, yielding a gummy extract of 342 g with a wet-to-extract weight of 14.6%. This extract was stored at -20 °C in a refrigerator and subsequently lyophilized in a freeze dryer, yielding 320 g of dried powder with a wet-to-dried yield of 13.7%. Partitioning was performed between methanol and hexane in a separatory funnel.

The methanol part (167 g) was reserved for future analysis. While the hexane fraction (approximately 70 g) was subjected to column chromatography (7 × 20 cm column packed with 500 g silica gel (40–60 μm)) using a gradient of hexane: ethyl acetate as the mobile phase: (100:0, 1.5 L, ST-7-1(52.1 g); h:3, 1.5 L, ST-7-2(7.3 g); 92:8, 2 L, ST-7-3(6.9 g); 88:12, 2 L, ST-7-4(1.45 g); 80:20, 1 L, ST-7-5(0.57 g)). The first fraction, ST-7-1, was oily and submitted for GC-MS analysis. Fractions ST-7-2 and ST-7-3, which have the same TLC profiles, were developed in hexane: ethyl acetate (9:1) as the solvent and cerium sulphate (1% in 10% sulphuric acid) as the TLC reagent,

and then combined. These fractions were combined and further purified using an open column (2 × 80 cm; 40–60 µm; 106 g silica gel) with a dichloromethane: ethyl acetate gradient: 100:0, 300 mL, discarded; 97:3, 300 mL, ST-11-1; 95:5, 300 mL, ST-11-2; 90:10, 300 mL, ST-11-3. After checking the primary H-NMR spectra of fractions, ST-11-1, with a steroid pattern, was selected and purified on Sephadex LH-20 gel chromatography with dimensions of 100 × 2 cm, using hexane: acetone: methanol (30:10:60). Final purification was carried out by HPLC on a YMC silica column (20 × 250 mm, 5 µm). The mobile phase consisted of hexane and ethyl acetate (85:15, v/v) at a flow rate of 3 mL/min. The system used was a semi-preparative Waters 600 HPLC equipped with a refractive index detector. The injection volume was 2 µL, and the column temperature was kept at 25 °C. Fractions corresponding to the target peaks were collected at a retention time of 45 minutes. This gave us compound 1 (1.7 mg) and compound 2 (3.4 mg).

Similarly, ST-11-2 was subjected to gel chromatography under the same conditions, yielding compound 3 (1.8 mg) and compound 4 (1.2 mg).

GC Mass analysis

For GC-MS analysis of the extract, it should be volatilized using silylating agents before injection. Bis(Trimethylsilyl) Trifluoroacetamide (BSTFA)+ TMCS (99+1) is a valid procedure for the determination of fatty acids by the GC-MS system, as reported by Jialin Du and co-workers.[11,12] With some modifications, 10 mg of the dried extract was taken into a small capped glass vial. BSTFA + TMCS (99+1, 50 µL) was added, and the mixture was heated for 1 hour at 80 °C. After evaporation of the remaining derivatization agent by N_2 gas, 1 mL hexane was added and injected into GC-MS for analysis on an HP-5 column (30 m, 0.25 mm, 0.25 µm) with column temperature program of 150 °C (Hold 4 min) ramping at 4 °C/min to 300 °C (Hold 5 min). The flow rate was set to 1 mL/min, the mass ionization voltage to 70 eV, and the mass ionization and quadrupole temperatures to 230 °C and 150 °C.

Antibacterial, anti-biofilm, and anti-efflux pump activities

Collection and identification of microbial isolates and microbroth dilution of colistin

A. baumannii was initially isolated from samples collected in the Intensive Care Units of Alzahra University, Isfahan, in 2023. After confirming *A. baumannii* by the Microbiology Department, Isfahan University of Medical Sciences, the presence of the *blaOXA-51-like* gene was examined for genetic identification. Antimicrobial susceptibility tests were performed according to the CLSI model, and the minimum inhibitory concentration (MIC) of colistin was determined using the microbroth dilution method in Mueller–Hinton broth (MHB). Serial dilutions of colistin and samples were prepared from 256 to 0.5 µg/mL. The bacterial suspension was standardized and added to the wells to reach a final concentration of approximately 10^5 CFU/mL. The plates were incubated at 37 °C for 16 h, and MIC values were determined. [13,14]

Selection of colistin-resistant bacteria

The susceptibility or resistance of the isolated bacteria to colistin was evaluated in both the presence and absence of the efflux pump inhibitor carbonyl cyanide 3-chlorophenylhydrazone (CCCP) (Sigma–Aldrich, St. Louis, MO, USA). Colistin was applied at concentrations ranging from 0.25 to 256 µg/mL in Mueller-Hinton broth plates. CCCP was then added to the respective plates to a final volume of 100 µL. The MIC of colistin was determined under both conditions. A fourfold or greater increase in MIC values following the addition of CCCP indicated the presence of an efflux pump mechanism. Bacterial strains exhibiting this mechanism were selected as colistin-resistant isolates in this study. [15]

Antibacterial activities

For antibacterial assays, the bacterial suspension was first adjusted to 0.5 McFarland turbidity in LB broth and subsequently diluted 1/1000, yielding a final turbidity of approximately 5.0×10^4 CFU/mL**.** For agar well diffusion assays, the bacterial suspension was diluted to OD600 = 0.2**,** spread uniformly on agar plates, and wells of 6 mm diameter were prepared. Then, 50 µL of compounds 1-3 at concentrations ranging from 62.5 to 2000 µg/mL were added to the wells, and the plates were incubated at 37 °C for 24 h. The diameter of the inhibition zones was subsequently measured. Colistin and PBS were used as positive and negative controls, respectively.[15] Compound 4 was not assayed because it was identified after the completion of the biological tests, and its quantity was less than 1 mg, which was insufficient for biological evaluation.

The MIC values of compounds 1-3 were determined using the broth microdilution method with two-fold serial dilutions ranging from 2000 to 62.5 µg/mL. In each well, 100 µL of the tested compound or colistin and 5 µL of bacterial inoculum were added and incubated at 37 °C for 24 h. Absorbance was measured at 595 nm, and MIC values were determined. Experiments were performed in triplicate, and the results were expressed as mean ± SD. The positive control contained bacteria with medium, while the negative control contained only medium. [16]

$$\%\text{anti} - \text{bacterial activities} = \frac{(\text{OD Positive control} - \text{OD tested compounds})}{(\text{OD Positive control})} \times 100$$

Anti-biofilm activities:

Antibiofilm activity was determined using the crystal violet method in 96-well plates. For this assay, 100 µL of each bacterial strain suspension was added to the wells and incubated at 37 °C for 72 h to allow biofilm formation. The culture medium was removed, and the wells were washed with PBS (pH 7.2). The formed biofilms were treated with two-fold serial dilutions of the samples ranging from 1000 to 62.5 µg/mL and incubated at 37 °C for 48 h. The wells were then washed with PBS, fixed with ethanol for 30 min, and stained with 0.1% crystal violet. After washing,

absorbance was measured at 590 nm. The experiments were performed in triplicate, and the results were expressed as mean ± SD. A placebo (medium without active compound) was used as the control representing maximum biofilm formation.

$$\%\text{anti}-\text{biofilm activities}=\frac{(\text{OD control}-\text{OD tested compounds})}{(\text{OD control})}\times 100$$

The ethidium bromide cartwheel method to evaluate the efflux pump activity

The agar-ethidium bromide cartwheel method was used to evaluate the effect of the bacteria's efflux pump on inhibitory activity. To accomplish this, ethidium bromide was added at a concentration of 1 µg/mL to Müller-Hinton agar plates, followed by inoculation of the bacteria that were treated with compounds 1-3 in their MIC concentrations, a placebo, alongside a negative control (*A. baumannii* ATCC19606) with no efflux pump in a cartwheel pattern (placing samples from the edge of the plate towards the center in a straight line which facilitated visualization of fluorescence differences). The plates were then incubated at 37°C for 24 hours to allow bacterial growth and efflux pump activity. After incubation, the plates were examined under UV light using the Uvitec Cambridge gel documentation system. Fluorescence intensity is associated with ethidium bromide accumulation, which binds to DNA in cells. Efflux pump activity expels it from bacteria and leads to lower fluorescence. It was excited at 530 nm, and fluorescence emission was measured at 600 nm with two replicates. [17]

Real-time PCR assay to measure MexB efflux pump gene expression

To determine the effects of the samples on the expression of the MexB efflux pump gene in *A. baumannii*, we used the PCR (qRT-PCR) method. First, RNA was extracted from bacterial cells using an RNA extraction kit (Cinnagen, Iran). Complementary DNA (cDNA) was synthesized according to the manufacturer's instructions.

For quantitative reverse transcription PCR (qRT-PCR), the ABI system (Applied Biosystems StepOne Plus™, USA) was used. Thermocycling conditions included an initial denaturation step at 95°C for 10 minutes, followed by 40 cycles of 15 seconds each at 95°C and 60 seconds at 54°C. We used the 16S rRNA gene as an internal control, and tests were done three times. Finally, the standard 2-ΔΔCT method was used for calculations. The primers used were designed according to Table 1. [18]

Table 1. Sequences of primers used in the Real-time PCR assay to measure the MexB efflux pump gene expression

Primers	Sequence 5′ → 3′	Length products (bp)	Reference
MexB	F: "CAACATCCA GGACCCACTCT" R: "AGGAAATCT GCACGTTCTGC"	167	[19]
16 SrRNA	F: "ATGTTGGGT TAAGTCCCG" R: "CTAGCGATT CCRRCTTCA"	256	[20]
$bla_{OXA\text{-}51\text{-}like}$	F: "TAATGCTTT GATCGGCCTTG" R: "TGGATTGCA CTTCATCTTGG"	353	[21]

Molecular docking study

Molecular docking studies were performed to assess the binding affinity of the tested compounds within the active site of the MexB efflux pump. The AutoDock software package was utilized to perform these calculations. The crystal structure of the MexB protein complexed with a known efflux protein inhibitor (EPI), identified by PDB ID: 3W9J, was obtained from the RCSB Protein Data Bank. Using Accelrys DS Visualizer 3.5, the co-crystallized EPI and all extraneous components, such as water and maltoside molecules, were eliminated in preparation for protein analysis. [22]

All missing hydrogen atoms were added, and after determining the Kollman united atom charges, nonpolar hydrogens were merged with their corresponding carbons using AutoDock tools. The three-dimensional structures were subsequently developed and optimized for ligand preparation using the Polak-Ribiere conjugate gradient algorithm alongside the PM3 semi-empirical method in HyperChem. After that, additional modifications were applied to these optimized structures with AutoDock tools, generating PDBQT files for each ligand. The primary modifications involved (a) computing partial charges using the Gasteiger-Marsili method, (b) incorporating polar hydrogens and consolidating nonpolar hydrogens, and (c) determining the center of gravity of the molecule (root) and counting the number of rotatable bonds. A grid map composed of 70 × 70 × 70 points, with a spacing of 0.375 Å between points, was used for all docking processes. Given that the position of the co-crystallized inhibitor in the MexB binding site was already known, the grid box center was aligned with the centroid of the bound inhibitor within the active site (X: 34.124; Y: 16.298; Z: -58.712), which roughly encompasses the center of the MexB binding pocket. [23] The Receptor Grid file was formatted in gpf. For each ligand, 100 independent docking attempts were performed utilizing the LGA search algorithm to find the global optimal binding position. This process commenced with an initial population of 150 randomly generated individuals, while all other run parameters were set to their default values. A cluster analysis was then performed with a tolerance of 2 Å or less in positional root-mean-square deviation to categorize the closest ligand conformations, with the original ligand coordinates serving as the reference structure. For the validity of the process, the co-crystallized inhibitor was retrieved from the X-ray complex and re-docked, and the best pose of the re-docked ligand was superimposed onto its X-ray counterparts in the 3W9J structure. In conclusion, the ligands' docking outcomes, including docked poses, free binding energies, and inhibition constants (Ki), were evaluated using AutoDockTools. [24]

In silico ADMET (absorption, distribution, metabolism, excretion, and toxicity) study

Studies on ADMET screening are essential for effective

drug development. Numerous drug candidates do not succeed due to unfavorable ADMET characteristics, including inadequate bioavailability and elevated toxicity. This research involved assessing the physicochemical properties and drug-likeness of the compounds tested using an online tool called SwissADME (http://swissadme.ch/).

Furthermore, the ADMETsAR database (http://lmmd.ecust.edu.cn/admetsar1/) was used to evaluate pharmacokinetic attributes and toxicity. [25]

Statistical analysis

All data are expressed as mean ± standard deviation (SD). Statistical analyses were performed using GraphPad Prism (version 8.4.3). One-way analysis of variance (ANOVA) was used to compare the mean of each treatment group with that of the control group. Statistical significance was indicated as follows: "*" $P < 0.05$, "**" $P < 0.01$, and "***" $P < 0.001$.

Results

Identification of components

The hexane fraction of the acetone extract of *S. tenuispiculatum* was submitted to repeated normal-phase chromatography, yielding four steroidal compounds 1-4. Compound **1** showed positive ESI-mass at *m/z* 427[M+H]$^+$ in agreement with $[C_{30}H_{51}O]^+$ molecular formula. The NMR spectra resembled steroid structure with thirty carbons including seven methyl groups: three singlets with δ_H 0.66 (singlet, H_18), 1.01 (singlet, H_19), 0.90 (singlet, H_29), four doublets with δ_H 1.25 (doublet, overlapped, H_21), 0.95 (doublet, overlapped, H_27), 0.94 (doublet, overlapped, H_28), 0.86 (doublet, J = 6.6, H_26), nine methylene groups including a pair of doublet of doublets in the upfield area at δ_H 0.45 (doublet of doublets, J = 9.1, 4.3, H_30b), and -0.13 (doublet of doublets, J = 4.3, 5.7, H_30a), characteristic of methylene at a cyclopropane ring, ten methines including one double bond at δ_H 5.35 (broad doublet, J = 5.0 Hz, H_6), and one oxygenated at δ_H 3.50 (m, H_3), and four quaternary carbons including one double bond at δ_C 140.92 (C5), which resembled gorgasta-5-en-3-ol. [26] Gorgosterol was previously extracted from other soft corals, including *Alcyonium molle*, *Sarcophyton glaucum*, and *Sinularia compressa*. [27-29] Compound **2** exhibited positive ESIMS at *m/z* 401[M+H]$^+$ indicative of $C_{28}H_{47}O$ with NMR signals for a total of 28 carbon atoms with six methyl groups consisting of two singlets at δ_H 1.03 (singlet, H_19), and 0.70 (singlet, H_18), four doublets at δ_H 0.94 (*d*, J = 6.4, H_21), 0.88 (*d*, J = 6.8, H_27), 0.82 (*d*, J = 2.8, H_26), 0.80 (*d*, J = 2.8, H_28), ten methylene groups, nine methines including one double bind at δ_H 5.35 (*dt*, J = 5.8, 2.0 Hz, H_6), and one oxygenated at δ_H 3.53 (multiplet, H_3), and three quaternary carbons including one olefin at δ_C 141.23 (C5). It was in agreement with the data of ergosta-5-en-3β-ol. [30] Compound **3** was detected as a positive ESI peak at m/z 429 [M+H],$^+$ consistent with $C_{28}H_{45}O_3$. The ^{13}C NMR and DEPT spectral analysis revealed the presence of 28 carbon atoms, which included six methyl groups, seven methylene groups, eleven methine carbons (four of which are olefins, and one is oxygenated), along with four quaternary carbons (two oxygenated). Additionally, the ^{1}H NMR spectrum displayed two disubstituted double bonds, with one pair of cis-oriented protons appearing downfield at δ_H 6.51(doublet, J = 8.5, H_7), 6.23(doublet, J = 8.5, H_6), and another *trans* pair at δ_H 5.16 (*dd*, J = 15.2, 7.5 Hz, H_23), 5.22 (*dd*, J = 15.3, 8.1, H_22), one hydroxymethine at δ_H 3.97 (multiplet, H_3), two singlet methyls at δ_H 0.88 (singlet, H_19), 0.82 (singlet, H_18), along with four doublet methyls at δ_H 0.90 (doublet, J = 6.9, H_28), 0.84 (doublet, J = 1.84, H_27), and 0.81 (doublet, J = 3.6, H_26) which was similar with data of 5,8α-epidioxyergosta-6,22*E*-dien-3-ol. [29] Compound 4 showed a positive ESI mass of *m/z* 431[M+H],$^+$ indicative of the molecular formula of $C_{28}H_{47}O_3$, based on ^{13}C NMR signals composed of 28 carbons similar to those of compound **3** except for the lack of a double bond at C-22. These data were agreement with the structure of 5,8-epitaxy-5,8α-ergosta-6-en-3-ol. [31]

Spectral data of isolated compounds

Four steroids from gorgastane and ergostane types were isolated with the following spectral data: (Figure 1).

Gorgasta-5-en-3β-ol (1): ^{1}H NMR (400.15, CDCl3): 5.35 (*bd*, 5.0 Hz, H_6), 3.50 (*m*, H_3), 1.25(*d*, overlapped, H_21), 1.01 (*s*, H_19), 0.95 (*d*, overlapped, H_27), 0.94 (*d*, overlapped, H_28), 0.90 (*s*, H_29), 0.86 (*d*, 6.63, H_26), 0.66 (*s*, H_18), 0.45 (*dd*, 4.3, 9.11, H_30b), -0.13 (*dd*, 5.7, 4.3, H_30a); ^{13}C NMR (100.62, $CDCl_3$): 140.92 (C_5), 121.89 (C_6), 71.98 (C_3), 58.08 (C_17), 56.78 (C_14), 50.96 (C_24), 50.31 (C_9), 42.93 (C_13), 42.46 (C_4), 40.01 (C_12), 37.40 (C_1), 36.66 (C_10), 35.44 (C_20), 32.29 (C_25), 32.19 (C_22), 32.05(C_8) 32.12 (C_7), 31.91 (C_8), 31.50 (C_2), 29.85 (C_16), 28.39 (C_23), 25.95 (C_15), 24.70 (C_21), 22.34 (C_26), 21.68 (C_30), 21.45 (C_27), 21.32 (C_11), 19.55 (C_19), 15.60 (C_28), 14.43 (C_29), 12.05 (C_18). Pos ESIMS: m/z 427 [M+H]$^+$(Figure S1-S5). [26]

Ergosta-5-en-3β-ol (2): ^{1}H NMR (400.15, $CDCl_3$): δ_H 5.35 (*dt*, 5.8, 2.0, H_6), 3.53 (*dddd*, 9.5, 9.5, 4.6, 4.6, H_3), 1.03 (*s*, H_19), 0.94 (*d*, 6.4, H_21), 0.88 (*d*, 6.8, H_27), 0.82 (*d*, 2.8, H_26), 0.80 (*d*, 2.8, H_28), 0.70 (*s*, H_18). ^{13}C NMR (100.62, $CDCl_3$): 141.23 (C_5), 122.18 (C_6), 72.27 (C_3), 57.22 (C_14), 56.46 (C_17), 50.60(C_9), 42.77(C_4), 42.77 (C_13), 40.23 (C_12), 39.53 (C_24), 37.72 (C_1), 36.97 (C_10), 36.65 (C_20), 34.19 (C_22), 32.37 (C_23), 32.37 (C_8), 32.13 (C_7), 31.93 (C_25), 31.04 (C_2), 28.66 (C_16), 24.76 (C_15), 21.55 (C_11), 20.99 (C_21), 19.86 (C_19), 19.36 (C_27), 18.06 (C_26), 15.91 (C_28), 12.32 (C_18). Pos ESIMS: m/z 401 [M+H]$^+$ (Figure S6-S10).[30]

5,8-Epidioxy-5, 8α-ergosta-6, 22E-dien-3β-ol (3): ^{1}H NMR (400.15, $CDCl_3$): δ_H 6.51 (*d*, 8.5, H_7), 6.23 (*d*, 8.5, H_6), 5.22 (*dd*, 15.3, 8.1, H_22), 5.16 (*dd*, 15.2, 7.5, H_23), 3.97 (*dddd*, 11.45, 11.45, 5.06, 5.06, H_3), 0.99 (*d*, 6.1 H_21), 0.90 (*d*, 6.9, H_28), 0.88 (*s*, H_19), 0.84 (*d*, 1.84, H_27), 0.82 (*s*, H_18), 0.81 (*d*, 3.6, H_26); ^{13}C NMR (100.62, CDCl3): 135.56 (C_6), 135.25 (C_22), 132.44 (C_23), 130.89 (C_7), 82.29 (C_5), 79.56 (C_8), 66.61 (C_3), 56.32 (C_17), 52.81 (C_14), 51.20 (C_9), 44.69 (C_13), 43.91 (C_24), 39.90 (C_20), 39.47 (C_12), 37.09 (C_4), 37.05 (C_10), 34.82

(C_1), 33.20 (C_25), 30.24 (C_2), 28.81 (C_16), 23.54 (C_11), 21.02 (C_21), 20.77 (C_15), 20.10 (C_26), 19.79 (C_27), 18.32 (C_19), 17.70 (C_28), 13.01 (C_18). Pos ESI-mass: *m/z* 429 $[M+H]^+$ (Figure S11-S13).[29]

5,8-Epidioxy-5, 8α-ergosta-6-en-3β-ol (4): ^{1}H NMR (400.15, $CDCl_3$): δ_H 6.49 (*d*, 8.1, H_7), 6.24 (*d*, 8.2, H_6), 3.96 (*dddd*, 10.95, 10.95, 5.09, 5.09, H_3), 1.00(*d*, 6.5, H_21), 0.92 (*d*, 7.6, H_28), 0.88 (*s*, H_19), 0.84 (*d*, 3.48, H_27), 0.82 (*s*, H_18), 0.80 (*d*, 3.37, H_26); ^{13}C NMR (100.62, CDCl3): 135.36 (C_6), 130.72 (C_7), 82.10 (C_5), 79.37 (C_8), 66.43 (C_3), 56.34 (C_17), 51.02 (C_14), 44.50(C_9), 43.94 (C_13), 42.72 (C_24)39.37 (C_20), 39.29 (C_12), 38.97 (C_10), 36.87 (C_4), 34.64 (C_1), 33.14 (C_25), 32.52 (C_22), 30.06 (C_23), 29.65 (C_2), 25.48 (C_16), 23.35 (C_11), 20.45 (C_26), 20.82 (C_21), 20.58 (C_15), 19.57(C_27), 18.11 (C_19), 17.50 (C_28), 12.57 (C_18).

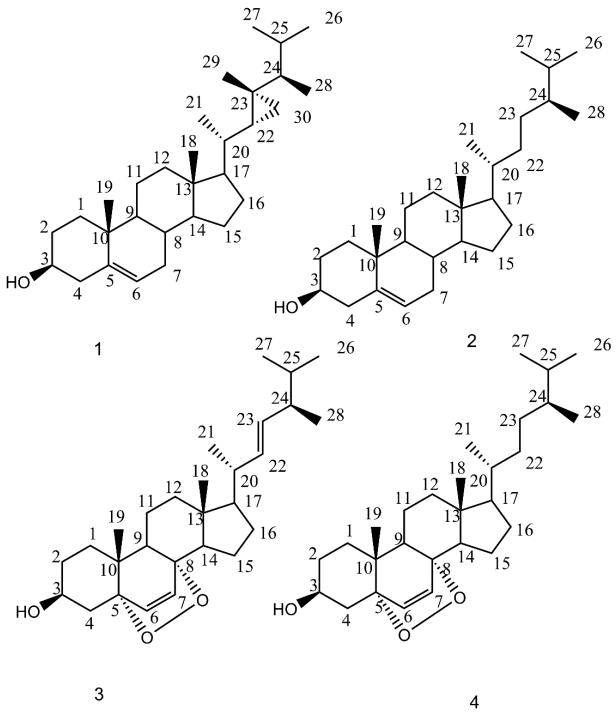


Figure 1. Isolated steroids from Sarcophyton tenuispiculatum

Pos ESI-mass: *m/z* 431 $[M+H]^+$ (Figure S14-S16).

GC Mass analysis

GC-MS analysis was performed on the oily portion of the hexane fraction. The results revealed the presence of long-chain ester alcohols including Lauric acid hexadecyl ester (4.17%), Myristic acid hexadecyl ester (12.23%), cis-9-Hexadecenoic acid hexadecyl ester (3.75%), Palmitic acid hexadecyl ester (30.94%), and Palmitic acid octadecyl ester (11.88%), as well as one sesquiterpene: Alloaromadendrene (4.17%), and two unidentified cembrane diterpenes (21.09%) were detected (Table 2). The designation "unknown cembrane diterpenes" in Table 2 indicates that, although GC-MS detected these compounds, their exact structural identities have not yet been determined. As a result, they remain classified as unknown pending further chromatographic separation and NMR characterization(Table 2).

Antibacterial, anti-biofilm, and anti-efflux pump activities

Antibacterial and anti-biofilm activity

The first three isolated steroids (compounds 1-3), along with colistin as a standard drug, were evaluated against colistin resitant *A. baumannii* using the CLSI protocol. Compound 1 exhibited the more antibacterial activity, with an MIC of 500 µg/mL, followed by compounds 2 and 3 with MICs of 1700 and 2000 µg/mL, compared with colistin with a MIC of 32000 µg/mL.

Compound 1 also exhibited an MBC of 850 µg/mL. In contrast, the other compounds did not reach their MBCs within the tested concentration range of 8 to 2000 µg/mL.

In the biofilm formation assay, compounds 1, 2, and 3 reduced biofilm formation by 79 ± 6.4 %, 78 ± 7.1 %, and 69 ± 5.8 %, compared to the placebo in the untreated control group (Table 3). Compound 4 was not tested because the isolated amount was insufficient for reproducible biological assays; therefore, biological conclusions are limited to compounds 1–3.

Table 2. Chemical composition of ST-7-1 (oily part of hexane fraction) of *Sarcophyton tenuispiculatum* identified by GC-MS analysis

Compounds		Molecular formula	RI (ref.)	Retention times (min)	Identification method RI (exp.), Mass (quality)	TIC (percent)	References
1	Alloaromadendrene	$C_{15}H_{24}$	1495	4.302	RI (1501), Mass (96%)	4.17	[32]
2	Unknown cembrane by GC-MS	-	-	12.23	RI (2180), Mass	12.23	-
3	Unknown cembrane by GC-MS	-	-	12.74	RI (2216), Mass	8.86	-
4	Lauric acid, Hexadecyl ester	$C_{28}H_{56}O_2$	2951	24.90	RI (2950), Mass (92%)	2.94	[33]
5	Myristic acid, Hexadecyl ester	$C_{30}H_{60}O_2$	3148	28.15	RI (3153), Mass (99%)	10.63	[33]
6	cis-9-Hexadecenoic acid, Hexadecyl ester	$C_{32}H_{62}O_2$	3328.7	30.93	RI (3335), Mass (83%)	3.75	[33]
7	Palmitic acid, Hexadecyl ester	$C_{32}H_{64}O_2$	3347	31.29	RI (3359), Mass (99%)	30.94	[33]
8	Palmitic acid, octadecyl ester	$C_{34}H_{68}O_2$	3546.5	34.17	RI (3551), Mass (95%)	11.88	[33]
		Terpenoids				25.26	
		Fatty acids and derivatives				60.14	
		Minor Compounds less than 1 %				14.6	

RI: Retention indices; Rt: Retention time; TIC: Total ion count.

Ethidium bromide-agar cartwheel method to evaluate the efflux pump activity

The results presented in Figure 2 compare the efflux pump activity of compounds 1-3 in *A. baumannii,* using control groups with and without an efflux pump function. Compound 1 ($P<0.001$), similar to the control group with no efflux pump (negative efflux pump control), showed a significantly increased fluorescence intensity versus the positive efflux control group ($P<0.001$) due to its inhibitory effect on the AdeABC efflux pump. Compounds 2 ($P=0.136$) and 3 ($P=0.014$) did not show significant fluorescence intensity.

Real-time PCR of the MexB gene

Real-time PCR was conducted to assess the impact of compounds 1–3 on the expression of the MexB efflux pump gene in colistin-resistant *A. baumannii*. The results indicated the significant downregulation of the MexB efflux pump gene following treatment with compounds 1 ($P=0.000$) and 2 ($P=0.011$) (Figure 3). In contrast, treatment with compound 3 ($P=0.449$) did not produce a statistical difference compared to the control group, as resistant bacteria (* $P<0.05$ and *** $P<0.001$).

Molecular docking of compounds 1–3

In silico docking experiments aimed to evaluate the steroids' capability to engage with the binding site of the MexB efflux pump at the molecular level. The results, summarized in Tables 4 and 5, include calculated values for free binding energy (ΔG_bind), various energy components at the optimal docked positions, and favorable interactions with key amino acid residues located within the active site of MexB.

Figures 4 and 5 present a 3D portrayal of the co-crystallized or best-predicted ligand's binding mode in the active site of the MexB DBP protein. These figures highlight the amino acid residues involved in hydrophobic, π–π, and hydrogen bond interactions with the ligands in the docked pocket.

Notably, the binding energies of compounds 1–3 (–11.06 to –8.66 kcal/mol) were markedly lower than that of colistin (–7.31 kcal/mol), indicating stronger predicted affinity toward the MexB deep binding pocket. Among them, compound 1 exhibited the most favorable binding energy, exceeding that of colistin by approximately 3.7 kcal/mol. This enhanced affinity is consistent with the extensive

Table 3. Antibacterial and anti-biofilm activity of compounds **1-3** against colistin-resistant *A. baumannii* with efflux pump activity

	MIC (μg/mL)	**MBC** (μg/mL)	**Biofilm**
Compound 1	500	850 *	500 μg/mL (79% reduction)
Compound 2	1700	>2000	500 μg/mL (78% reduction)
Compound 3	2000	>2000	500 μg/mL (62% reduction)

*Only this sample at this concentration could eradicate the growth of bacteria.

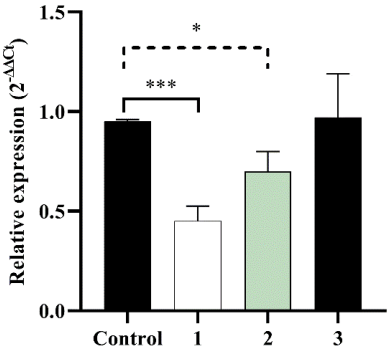


Figure 3. Real-time PCR of the MexB gene. The relative fold change in the MexB gene associated with the efflux pump was assessed after treatment with compounds 1-3 using quantitative real-time PCR. The examined genes' threshold cycle (CT) values were normalized against the 16S rRNA gene (* $P<0.05$ and *** $P<0.001$).

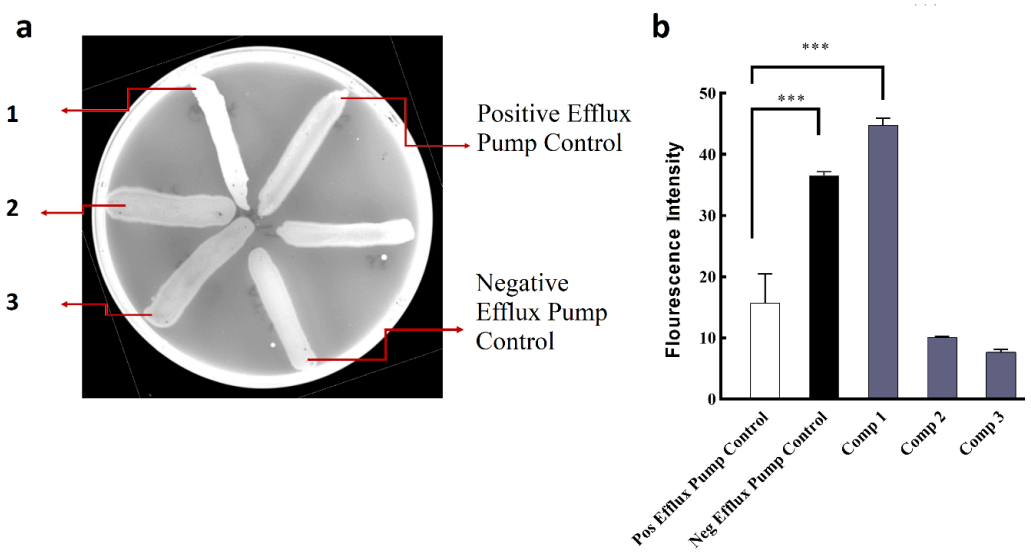


Figure 2. Ethidium bromide cartwheel assay. a: Ethidium bromide was added at a concentration of 1 μg/mL to Müller-Hinton agar plates and inoculated with compounds **1-3**, and a placebo (positive efflux pump control) on colistin-resistant clinical isolates (*A. baumannii* bacteria with efflux active pumps) alongside a control (negative efflux pump control) without efflux pump (*A. baumannii* ATCC19606) in a cartwheel pattern. b: Comparing the efflux pump activity of compounds **1-3** in *A. baumannii,* versus positive control group with efflux pump function and negative control without an efflux pump function (*** $P<0.001$).

hydrophobic interactions observed between compound 1 and key DBP residues and correlates well with its superior efflux pump inhibition and MexB downregulation observed experimentally (Table 4)

In silico ADMET study

The SMILES codes for compounds 1-4 are given in Table 6, in accordance with the Lipinski model, which is used for solubility and permeability prediction of small molecules.[34] These compounds exhibit drug-like properties (Table 6), with molecular weights below m daltons, hydrogen bond acceptor sites less than 10, HB donors less than 5, and MlogP values greater than 4.15. TPSA (Topological Polar Surface Area), a key factor influencing membrane permeability, ranged between 20–130 Å², which falls within the acceptable range according to admetSAR predictions (Table 7). These values suggest favorable gastrointestinal absorption and blood–brain barrier (BBB) penetration. The compounds also appear to be P-glycoprotein (P-gp) substrates, indicating potential accumulation within mitochondria. Therefore, their intracellular transport and cellular accumulation are influenced by mitochondria and efflux pump mechanisms. They are not predicted to be cytochrome 450 (1A2, 2C9, 2D6, and 2C19) inhibitors, although they may act as substrates for CYP450 3A4. They are also likely to be weak inhibitors of the hERG (ether-à-go-go-related gene) channel and are predicted to be non-carcinogenic.[35]

Table 4. The docking results illustrating the interaction between tested compounds and the reference ligand (colistin) at the MexB binding site (PDB ID: 3W9J) reveal significant findings.

Compd.	ΔG_{bind} (kcal/mol)	VHDE[a] (kcal/mol)	EE[b] (kcal/mol)	IE[c] (kcal/mol)	IC[d] (nM)
Compound 1	-11.06	-12.53	-0.03	-12.55	7.81
Compound 2	-10.68	-12.46	-0.01	-1247	14.79
Compound 3	-8.66	-1063	-0.12	-10.75	446.14
Colistin	-7.31	-17.42	-0.63	-18.05	4.36
Co-crystalized ligand	-10.67	-14.17	-0.68	-14.84	15.13

[a]VanderWaals-Hbond-Desolvation-Energy = VHDE. [b]Electrostatic Energy = EE. [c]Intermolecular Energy = IE. [d]Inhibition-Constant = IC

Table 5. Information regarding the interactions between the extracted steroids and the reference ligand (colistin) with the amino acid residues at the MexB binding site (PDB ID: 3W9J)

Tested compounds	Amino acid residues in the hydrophobic interactions	Amino acid residues in the hydrogen bond interactions	Amino acid residues in the pi interactions
Compound 1	LYS134, VAL571, PHE136, PRO326, PHE617, ALA290, PHE573, GLN176, MET630, TYR327, VAL139, PHE178, PHE610, VAL612, PHE615, PHE617, PHE628, PRO669	LEU672, GLY675	PHE628(sigma-pi)
Compound 2	ALA_{279}, VAL_{612}, THR6$_{11}$, V_{139}, PHE_{136}, PHE_{610}, LYS_{134}, PHE_{573}, PHE_{617}, PRO_{669}	GLY_{685}	PHE_{628}, PHE_{178} (sigma-pi)
Compound 3	GLY_{675}, LEU$_{67}$2, PHE_{617}, PHE_{136}, PHE_{573}, VAL_{139}, TYR_{327}, PHE_{628}, PHE_{610}, MET_{630}, PHE_{178}	LYS_{134}	–
Colistin	SER_{79}, GLY_{619}, ASN_{616}, GLU_{81}, GLU_{825}, PHE_{615}, PHE_{136}, VAL_{612}, ILE_{277}, THR_{130}	LYS $_{134}$, GLN $_{176}$, GLN_{46}, VAL $_{177}$, GLY $_{675}$	-
Co-crystalized ligand	ALA_{279}, VAL_{612}, VAL_{139}, PHE_{573}, TYR_{327}, PHE_{610}, PHE_{617}, PHE_{136}, PHE_{628}, PHE_{615} PRO_{326}, MET_{630}, VAL_{571}	LYS_{151}	VAL_{139}, ILE_{277}, PHE_{615}(sigma-pi) ARG_{620}(cation-pi) PHE_{628}, PHE_{178}(pi-pi)

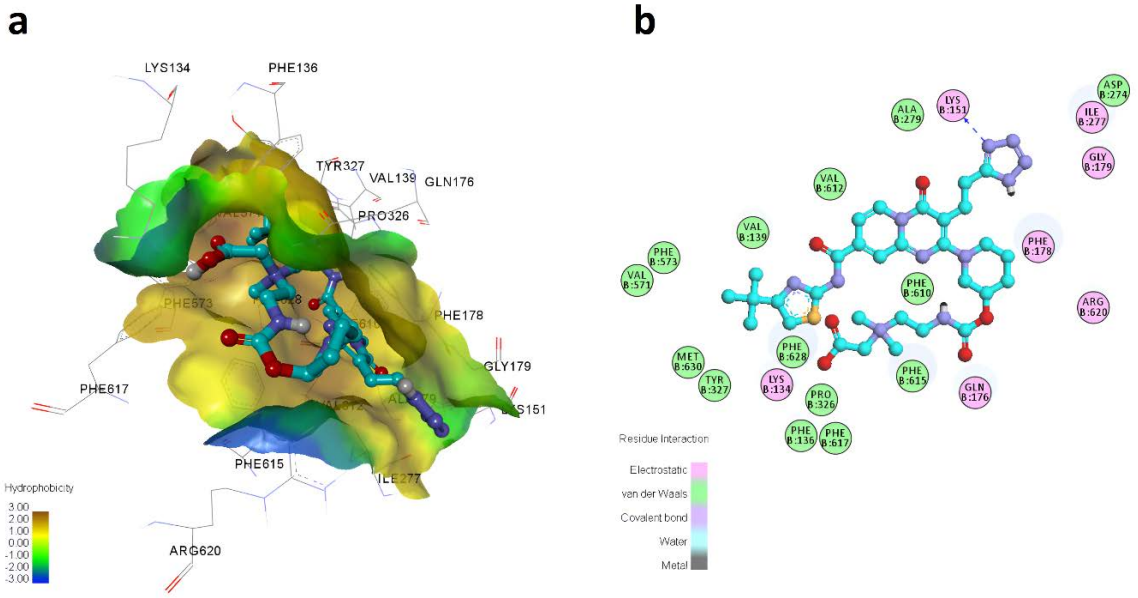


Figure 4: (a) A three-dimensional representation of the proposed binding mode of the co-crystallized ligand within the MexB drug-binding pocket (DBP). The ligand is depicted using a ball-and-stick model with distinct colors representing different elements, while stick models indicate the primary interacting amino acid residues. (b) A two-dimensional illustration showing the interaction between the optimal redocked pose of the co-crystallized ligand and key amino acid residues in the DBP of MexB.

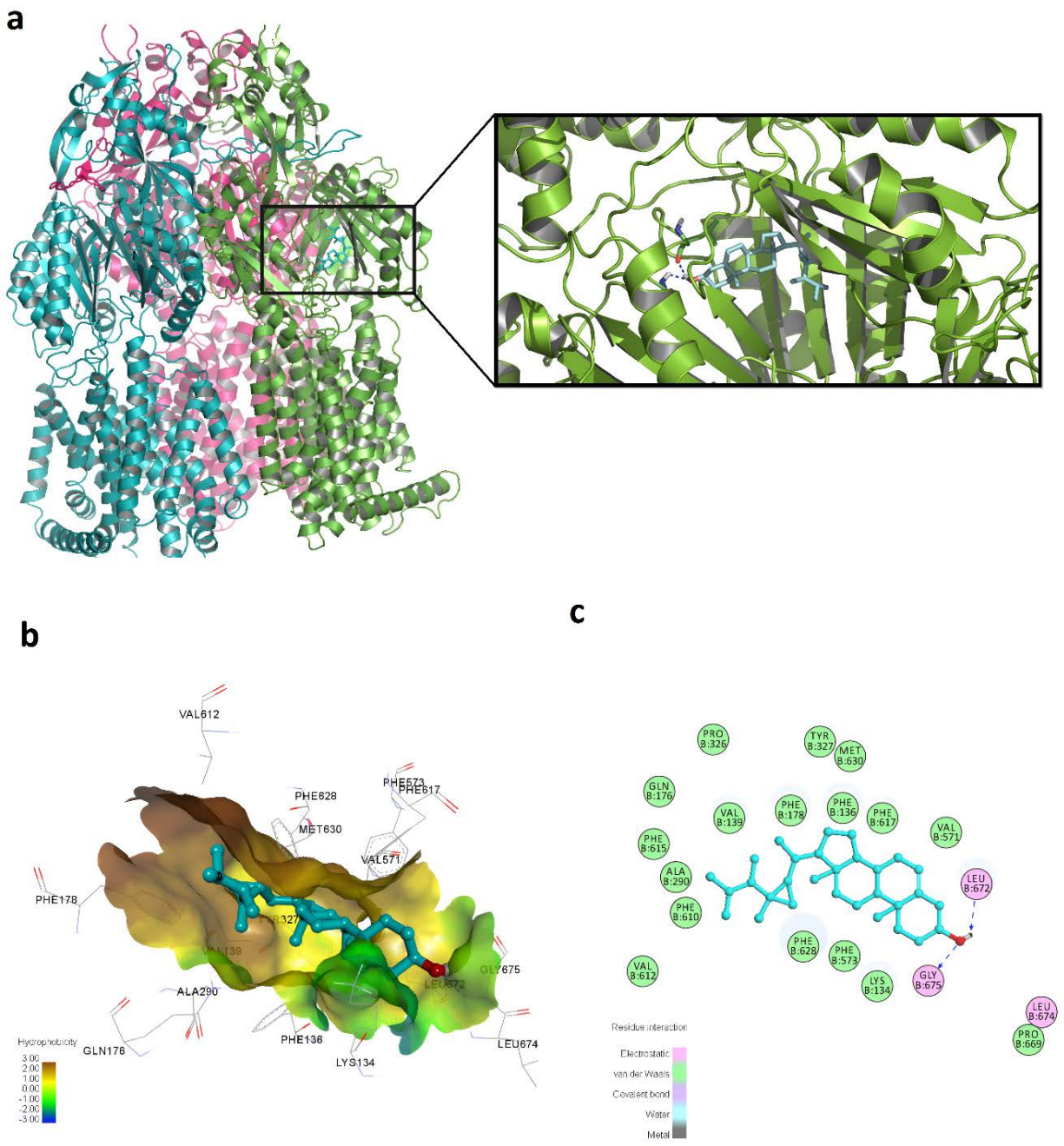


Figure 5: Predicted binding site of compound **1** inside the MexB protein as found by molecular docking studies. (a) Structure of the best-docked pose of ligand **1** in the MexB trimer, along with a close-up view of the ligand bound to the hydrophobic distal binding pocket (DBP) of MexB. Three MexB monomers are shown in green, blue, and pink ribbon models, and the ligand is represented as a cyan stick model. (b) 3D portrayal of the putative-binding mode of the ligand in the DBP of the MexB. The ligand is illustrated using a ball-and-stick model, featuring distinct colors for different elements, while stick representations highlight the primary interacting amino acid groups. (c) presents a two-dimensional illustration that shows the interaction between the ligand and essential amino acid residues in the DBP of MexB.

Table 6. Molecular Input Line Entry System (SMILES) codes of tested compounds

Compound	SMILES	HBA	HBD	MlogP	TPSA	Drug likeness (Lipinski)
1	CC(C)[C@@H](C)C1(C)C[C@@H]1[C@@H](C)C1CCC2C3CC=C4C[C@@H](O)CC[C@]4(C)C3CC[C@]12C	1	1	6.92	20.23 Å²	Yes, one violation: MLOGP>4.15
2	CC(C)[C@@H](C)CC[C@@H](C)C1CCC2C3CC=C4C[C@@H](O)CC[C@]4(C)C3CC[C@]12C	1	1	6.54	20.23 Å²	Yes, one violation: MLOGP>4.15
3	CC(C)[C@@H](C)\C=C\[C@@H](C)C1CCC2[C@]1(C)CCC1[C@@]3(C)CC[C@H](O)C[C@@]33OO[C@@]21C=C3	3	1	5.43	38.69 Å²	Yes, one violation: MLOGP>4.15
4	CC(C)[C@@H](C)CC[C@@H](C)C1CCC2[C@]1(C)CCC1[C@@]3(C)CC[C@H](O)C[C@@]33OO[C@@]21C=C3	3	1	5.54	38.69 Å²	Yes, one violation: MLOGP>4.15

Table 7. Pharmacokinetics and toxicity by AdmetSAR

Model	Compound 1	Compound 2	Compound 3	Compound 4
Absorption				
Blood–brain barrier	BBB permb+	BBB permb+	BBB permb+	BBB permb+
Human intestinal absorption	HIA+	HIA+	HIA+	HIA+
P-glycoprotein substrate	Substrate	Substrate	Substrate	Substrate
Distribution				
Subcellular localization	Mitochondria	Mitochondria	Mitochondria	Mitochondria
Metabolism				
CYP2C9 substrate	No-substrate	No-substrate	No-substrate	No-substrate
CYP2D6 substrate	No-substrate	No-substrate	No-substrate	No-substrate
CYP3A4 substrate	Substrate	Substrate	Substrate	Substrate
CYP1A2 inhibitor	No-inhibitor	No-inhibitor	No-inhibitor	No-inhibitor
CYP2C9 inhibitor	No-inhibitor	No-inhibitor	No-inhibitor	No-inhibitor
CYP2D6 inhibitor	No-inhibitor	No-inhibitor	No-inhibitor	No-inhibitor
CYP2C19 inhibitor	No-inhibitor	No-inhibitor	No-inhibitor	No-inhibitor
CYP3A4 Inhibitor	No-inhibitor	No-inhibitor	No-inhibitor	No-inhibitor
Toxicity				
hERG inhibition	Weak inhibitor	Weak inhibitor	Weak inhibitor	Weak inhibitor
AMES Toxicity	No-AMES toxic	No-AMES toxic	AMES toxic	AMES toxic
Carcinogens	No-carcinogens	No-carcinogens	No-carcinogens	No-carcinogens

hERG: human Ether-a-go-go-Related Gene; BBB permb: Blood–brain barrier permeability. These predictions are based on ADMET computational information and require experimental toxicity assays for confirmation.

According to admetSAR predictions presented in Table 7, steroids 1 and 2 were classified as non-mutagenic, showing no AMES toxicity. In contrast, steroids 3 and 4 were predicted to be AMES toxic, suggesting potential mutagenic effects. It is important to note that these predictions are based on computational ADMET modeling and require experimental toxicity assays for confirmation.

Discussion

Colistin, as one of the antibiotic choices for *A. baumannii*, is losing its effect due to the emergence of bacterial resistance mechanisms, including MexB efflux pump activity and biofilm formation in new *A. baumannii* strains. Recent studies have shown that certain steroids possess anti-efflux pump activity.[36] Consequently, *Sarcophyton tenuispiculatum*, a known source of steroidal compounds, was selected for investigation. Through phytochemical analysis, four steroids were isolated for the first time: gorgasta-5-en-3β-ol (1), ergosta-5-en-3β-ol (2), ergosterol peroxide (5,8-epidioxy-5,8-ergosta-6, 22-dien-3-ol) (3), and 5,8-epidioxy-5, 8-ergosta-6-en-3-ol (4).

Antibacterial assays in this research revealed that compound 1 exhibited the strongest activity among the tested compounds, with an MIC of 500 µg/mL. This discovery is essential because bactericidal agents are often preferred in clinical settings for treating severe infections where rapid bacterial clearance is critical. *A. baumannii's* ability to form biofilms significantly contributes to its persistence and resistance to therapy. The results from the microtiter plate assays offer important information regarding the compounds' biofilm-inhibiting properties. Compounds 1 (79%) and 2 (78%) showed the greatest decrease in biofilm formation. This level of biofilm reduction may be significant for controlling biofilm-associated infections because biofilms hinder antibiotic penetration and immune response, making infections more difficult to eradicate. [37] The present findings contribute to the understanding of potential therapeutic strategies against *A. baumannii* infections.Compounds 1 and 2 appear to be strong candidates for further development, particularly for their ability to reduce biofilm formation, a key aspect of managing chronic infections. Additionally, evaluating the toxicity and pharmacokinetics of these substances *in vivo* will be essential before considering any clinical use. The findings from the real-time PCR analysis indicated that compounds 1 and 2 downregulate the MexB gene, suggesting their potential as practical tools for combating antibiotic resistance by targeting bacterial efflux systems.

In a similar research, Tonny Loho et al. (2017) illustrate that combining antibiotics with efflux pump inhibitors can produce a synergistic effect, thereby decreasing the minimum inhibitory concentration (MIC) of antibiotics against *A. baumannii*. [38] In another study, Ranita Roy et al. (2018) presented evidence that employing agents that disrupt biofilm formation can significantly enhance the efficacy of antibiotic treatment for biofilm-associated *A. baumannii* infections. [39]

In agreement with this study, research by Wang et al. indicates that four steroid compounds of the gorgostane type (numbers 6, 12, 13, and 14) were isolated from the soft coral *Sarcophyton* sp. Their antibacterial and antifungal activities were evaluated using the agar diffusion method.

All four compounds showed some activity against bacteria and fungi. Compound 12 showed a potent antifungal effect, especially against *Microbotryum violaceum* (9.5 mm) and *Septoria tritici* (10.0 mm). Compound 13 was the most effective antifungal, with an 11.5 mm zone of inhibition against *Microbotryum violaceum*. These results indicate that specific structural components, such as the cyclopropane ring and the terminal double bond in the side chain, may contribute to improved biological activity. [40]

While Wang et al. reported gorgostane-type steroids with moderate antimicrobial activity, no assessment of efflux pump inhibition, gene expression modulation, or molecular interaction with resistance-related targets was performed. In contrast, the current work demonstrates that structurally related steroids from *S. tenuispiculatum*, particularly the gorgostane derivative 1, not only inhibit biofilm formation but also interfere with MexB efflux activity at phenotypic, transcriptional, and molecular levels. This mechanistic integration represents a significant advancement over earlier *Sarcophyton* studies.

In the *in-silico* study, the crystal structure of homotrimeric MexB bound to a Pyridopyrimidine-based efflux pump inhibitor (EPI) was used as a convenient target structure for molecular modeling studies. [41] According to this crystal structure, the MexB protein features two prominent binding sites: a proximal pocket and a distal cavity. Also referred to as the deep binding pocket (DBP). The DBP plays a significant role in antibiotic extrusion by the bacterial efflux pump. The hydrophobic nature of the MexB binding cavity has been reported as an essential factor for interaction with various EPIs.[42] As shown in Figure 4, the best re-docked pose of the pyridopyrimidine derivative was well inserted into the hydrophobic trap of the DBP encompassed by the amino acid residues $Ala_{279,}$ $Val_{612,}$ Val_{139}, Phe_{573}, Val_{571}, Met_{630}, Tyr_{327}, Phe_{628}, Pro_{326}, Phe_{617}, Phe_{136}, $Phe_{615,}$ and Phe_{610}. As a result, these residues primarily participate in expected hydrophobic interactions with the re-docked ligand. Residues Phe_{628} and Phe_{178} further contribute to the tighter binding of the inhibitor molecule through a π–π interaction with the pyridopyrimidine ring. The binding affinity of the ligand to DBP is also augmented by forming a hydrogen bond with Lys_{151}. After the validation, three proposed steroidal compounds were docked into the same DBP of MexB with superior free binding energy values (ranging from -11.06 to -8.66 Kcal.mol^{-1}) than the reference antibiotic, colistin (-7.31 Kcal.mol^{-1}), as shown in Table 4. This finding agreed with experimental data, highlighting the stronger binding affinity of the considered steroids towards the hydrophobic trap of DBP compared with colistin. In this regard, the hydrophobic residues (Pro, Leu, Phe, Val, and Ala) were mainly responsible for the EPI binding, consistent with previously reported studies. [43,44] Compound 1, with a binding energy of -11.06 kcal/mol, demonstrated the strongest affinity among the three steroids. The potential of this molecule to engage in more extensive hydrophobic interactions could contribute to an enhanced binding affinity toward the DBP, compared to the other studied molecules and colistin. The best-docked pose of this compound within the MexB binding cavity is illustrated in Figure 5. This steroid occupies the defined hydrophobic DBP in the MexB protein, forming a comprehensive network of hydrophobic interactions with key residues: Lys_{134}, Val_{571}, Phe_{136}, Ala_{290}, Phe_{573}, Gln_{176}, Met_{630}, Tyr_{327}, Pro_{326}, Val_{139}, Phe_{178}, Phe_{610}, Val_{612}, Phe_{615}, Phe_{617}, Phe_{628}, and $Pro_{669.}$ These interactions predominantly mediate its binding mode. This accommodation also enables the hydroxyl groups of the ligands to form favorable hydrogen-bond interactions with Leu672 and Gly675, thereby further stabilizing the ligands within the DBP. Based on these observations, molecular docking studies provide strong evidence that the examined steroids can interact with the hydrophobic DBP of MexB, thereby inhibiting drug expulsion through the bacterial efflux pump.

According to the predicted ADMET results, compounds 1 and 2 may have a less toxic profile, as they do not exhibit AMES toxicity. They show favourable absorption and distribution profiles with minimal metabolic issues. Compounds 3 and 4, although they exhibit encouraging pharmacokinetic properties, raise concerns about mutagenicity and should be developed with caution.

Based on ADMET studies, compounds 3 and 4 exhibit AMES toxicity, suggesting potential mutagenicity, raising concerns about their safety profile. AMES toxicity indicates a likelihood of DNA damage or mutations, which can contribute to genotoxic effects and increase the risk of carcinogenicity. While neither compound was classified as explicitly carcinogenic in the ADMET predictions, their mutagenic properties warrant further investigation, particularly through in vivo studies.

In the case of compounds 3 and 4, mutagenicity can lead to unwanted genetic changes and long-term toxicity risks. For these two compounds, structural modifications would be necessary to reduce these risks before clinical consideration.

However, the in vivo toxicity and pharmacokinetics of these compounds are still unclear, making animal models and clinical trials essential subsequent steps. Although compound 1 shows promise in targeting biofilm development and efflux pump mechanisms in drug-resistant *A. baumannii* infections, further pharmacological and toxicological evaluations are required.

Steroid substances found in *Sarcophyton* corals have an important ecological function, aiding the coral's survival and interactions with the surrounding environment. Among other roles, steroids in *Sarcophyton* corals function as chemical defences against predators and pathogens. These substances can deter herbivores and inhibit the proliferation of harmful bacteria and fungi. [45] Additionally, steroids may facilitate symbiotic relationships with other marine organisms, such as algae and bacteria, which are essential for nutrient cycling and energy production. The identified steroids are known for their potential biological activities, including anti-inflammatory, antimicrobial, and cytotoxic effects. For instance, gorgasta-5-en-3β-ol (compound 1) in *S. tenuispiculatum* might enhance

the organism's defence strategies against predators and pathogens, as these bioactive substances can repel herbivory and pathogen attacks. Likewise, ergosta-5-en-3β-ol (compound **2**) is known to influence immune responses across different organisms, potentially offering ecological benefits in the competitive marine ecosystem.

As limitation of study, although four steroids were isolated and structurally characterized, only compounds 1-3 were included in the biological assays. Compound 4 was obtained at a later stage of the isolation work, after completion of the primary biological experiments, and in insufficient quantity for reproducible antivirulant evaluation. Furthermore, the absence of a standard MexB efflux pump inhibitor as a positive control limited the strength of the assessment regarding the compounds' efflux pump inhibitory activity.

Conclusion

Accordingly, this study aims to isolate steroid compounds from the nonpolar fraction that can reduce biofilm formation and serve as potential MexB efflux pump inhibitors in colistin-resistant *Acinetobacter baumannii*. From the hexane fraction of the acetone extract, one gorgastane and three ergostane derivatives were isolated, alongside long-chain ester alcohols, alloaromadendrene, and two unidentified cembrane diterpenes identified by GC–MS spectrometry. Among these, gorgastanol (compound 1) notably decreased biofilm formation and inhibited the efflux pump activity, with real-time assays showing reduced MexB gene expression. Molecular binding studies confirmed its satisfactory affinity at the MexB pump's active site, as well as ADMET analysis revealed favorable absorption and distribution profiles with no predicted AMES toxicity.

Importantly, this work provides several novel contributions. To the best of our knowledge, this is the first report describing the isolation of these four steroids (1-4) from *S. tenuispiculatum* and their evaluation against colistin-resistant *A. baumannii*. Moreover, although steroidal metabolites have previously been associated with efflux pump modulation, this study provides the first evidence that a gorgostane-type steroid can inhibit the MexB efflux pump and suppress resistance-related mechanisms in this pathogen. The results also suggest a preliminary structure–activity relationship in which the gorgostane scaffold (compound 1) exhibits markedly stronger anti-efflux and antibiofilm activity than the ergostane derivatives. This enhanced activity may be related to the unique cyclopropane side-chain structure of the gorgostane skeleton, which enables stronger interactions within the hydrophobic MexB binding pocket. Collectively, these findings highlight marine steroids, particularly gorgostane derivatives, as promising antivirulence leads for addressing infections caused by colistin-resistant *A. baumannii*.

Acknowledgments

This research was part of a PhD thesis of Samin Mousavi and was funded by Isfahan University of Medical Sciences, Iran, Services Grants (No.3401376). This study was done under IR.MUIRESEARCH.1401.148 ethical code. we used previously collected clinical bacterial isolates with no associated patient identifiers.

Authors' Contribution

Conceptualization: Mustafa Ghanadian, Afsaneh Yegdaneh.
Formal Analysis: Arezoo Mirzaei, Hajar Sirous, Mohammad Bagher Majnooni.
Investigation: Samin Mousavi, Arezoo Mirzaei, Hajar Sirous, Mohammad Bagher Majnooni, Mustafa Ghanadian.
Methodology: Samin Mousavi, Melika Nazemi, Afsaneh Yegdaneh, Arezoo Mirzaei, Hajar Sirous, Mustafa Ghanadian.
Project Administration: Mustafa Ghanadian.
Resources: Mustafa Ghanadian, Afsaneh Yegdaneh.
Supervision: Mustafa Ghanadian, Afsaneh Yegdaneh.
Visualization: Arezoo Mirzaei, Hajar Sirous, Mohammad Bagher Majnooni, Mustafa Ghanadi.
Writing-Original Draft: Samin Mousavi, Mustafa Ghanadi.
Writing-Review & Editing: Samin Mousavi, Mustafa Ghanadian.

Competing Interests

The authors declare no conflicts of interest.

Data Availability Statement

The spectral data presented in this study are uploaded during submission as a supplementary file and are openly available for readers.

Declaration of using AI-assisted technology in the writing process

During the writing of the text, one of the authors, "MG," used Grammarly AI only to refine the English language. After using this tool/service, authors reviewed and edited the text again and accepted full responsibility for the content.

Ethical Approval

IR.MUI.RESEARCH.REC.1401.148.

Funding

This research was part of a PhD Thesis and was supported by Isfahan University of Medical Sciences, Iran, Services Grants (No.3401376).

Supplementary Files

Supplementary File contains Figure S1-S16.

References

1. Aratake S, Tomura T, Saitoh S, Yokokura R, Kawanishi Y, Shinjo R, et al. Soft coral *Sarcophyton* (Cnidaria: Anthozoa: Octocorallia) species diversity and chemotypes. PLoS One 2012;7(1): e30410. doi:10.1371/journal.pone.0030410
2. Brown KT, Barott KL. The costs and benefits of environmental memory for reef-building corals coping with recurring marine heatwaves. Integr Comp Biol 2022;62(6):1748-55. doi:10.1093/icb/icac074
3. Huang TY, Huang CY, Chen SR, Weng JR, Tu TH, Cheng YB, et al. New hydroquinone monoterpenoid and cembranoid-related metabolites from the soft coral *Sarcophyton tenuispiculatum*. Mar Drugs 2020;19(1):8. doi:10.3390/md19010008
4. Fahy S, O'Connor JA, Lucey B, Sleator RD. Hospital reservoirs of multidrug resistant *Acinetobacter* species-the elephant in the room! Br J Biomed Sci 2023;80:11098. doi:10.3389/bjbs.2023.11098
5. Talbot GH, Bradley J, Edwards JE Jr, Gilbert D, Scheld M, Bartlett JG. Bad bugs need drugs: an update on the development pipeline from the Antimicrobial Availability Task Force of the Infectious Diseases Society of America. Clin Infect Dis 2006;42(5):657-68. doi:10.1086/499819
6. Ayswarya K, Ibrahim R, Veetilvalappil VV, Bhat NB,

Aranjani JM. Virulence arsenal of *Acinetobacter baumannii*: mechanisms driving persistence and resistance. Arch Microbiol 2026;208(4):162. doi:10.1007/s00203-025-04668-7
7. Cevahir N, Demir M, Kaleli I, Gurbuz M, Tikvesli S. Evaluation of biofilm production, gelatinase activity, and mannose-resistant hemagglutination in *Acinetobacter baumannii* strains. J Microbiol Immunol Infect 2008;41(6):513-8.
8. Martí S, Rodríguez-Baño J, Catel-Ferreira M, Jouenne T, Vila J, Seifert H, et al. Biofilm formation at the solid-liquid and air-liquid interfaces by *Acinetobacter* species. BMC Res Notes 2011;4:5. doi:10.1186/1756-0500-4-5
9. Ahumada Topete VH, de Dios Sanchez KJ, Casas Aparicio GA, Hernandez Silva G, Lopez Vejar CE, Torres Espíndola LM, et al. Adverse events and drug resistance in critically ill patients treated with colistimethate sodium: a review of the literature. Infect Drug Resist 2023;16:1357-66. doi:10.2147/idr.S398930
10. Narimisa N, Keshtkar A, Dadgar-Zankbar L, Bostanghadiri N, Rouein Far Y, Shahroodian S, et al. Prevalence of colistin resistance in clinical isolates of *Pseudomonas aeruginosa*: a systematic review and meta-analysis. Front Microbiol 2024;15:1477836. doi:10.3389/fmicb.2024.1477836
11. Du J, Yang L, Wei K, Gong C, Gao J, Xu X. Determination of free fatty acids in rabbit plasma by GC-MS after trimethylsilylation derivatization. J Chin Pharm Sci 2020;29(6):411-21. doi:10.5246/jcps.2020.06.039
12. Tammekivi E, Vahur S, Kekišev O, van der Werf ID, Toom L, Herodes K, et al. Comparison of derivatization methods for the quantitative gas chromatographic analysis of oils. Anal Methods 2019;11(28):3514-22. doi:10.1039/c9ay00954j
13. Sisakhtpour B, Karbasizadeh V, Ebrahimi S, Hosseini NS, Mirzaee A, Shabani MS, et al. Investigation of the characteristics of multidrug-resistant (MDR) *Acinetobacter baumannii* lytic phage isolated from the intensive care unit. J Isfahan Med Sch 2019;37(528):564-71. doi:10.22122/jims.v37i528.11342
14. Mahon CR, Lehman DC. Textbook of Diagnostic Microbiology. Elsevier Health Sciences; 2022.
15. Majnooni MB, Ghanadian SM, Mojarrab M, Bahrami G, Mansouri K, Mirzaei A, et al. Antibacterial, antibiofilm, antiswarming, and antioxidant activities of flavonoids isolated from *Allium colchicifolium* leaves. J Food Biochem 2023;2023(1):5521661. doi:10.1155/2023/5521661
16. Przekwas J, Gębalski J, Kwiecińska-Piróg J, Wiktorczyk-Kapischke N, Wałecka-Zacharska E, Gospodarek-Komkowska E, et al. The effect of fluoroquinolones and antioxidans on biofilm formation by *Proteus mirabilis* strains. Ann Clin Microbiol Antimicrob 2022;21(1):22. doi:10.1186/s12941-022-00515-5
17. Fujiwara M, Yamasaki S, Morita Y, Nishino K. Evaluation of efflux pump inhibitors of MexAB- or MexXY-OprM in *Pseudomonas aeruginosa* using nucleic acid dyes. J Infect Chemother 2022;28(5):595-601. doi:10.1016/j.jiac.2022.01.003
18. Livak KJ, Schmittgen TD. Analysis of relative gene expression data using real-time quantitative PCR and the 2-ΔΔCT method. Methods 2001;25(4):402-8. doi:10.1006/meth.2001.1262
19. Abdelkarem FM, Abouelela ME, Kamel MR, Nafady AM, Allam AE, Abdel-Rahman IAM, et al. Chemical review of gorgostane-type steroids isolated from marine organisms and their 13C-NMR spectroscopic data characteristics. Mar Drugs 2022;20(2):139. doi:10.3390/md20020139
20. Aboutalebian S, Ahmadikia K, Fakhim H, Chabavizadeh J, Okhovat A, Nikaeen M, et al. Direct detection and identification of the most common bacteria and fungi causing otitis externa by a stepwise multiplex PCR. Front Cell Infect Microbiol 2021;11:644060. doi:10.3389/fcimb.2021.644060
21. Woodford N, Ellington MJ, Coelho JM, Turton JF, Ward ME, Brown S, et al. Multiplex PCR for genes encoding prevalent OXA carbapenemases in *Acinetobacter* spp. Int J Antimicrob Agents 2006;27(4):351-3. doi:10.1016/j.ijantimicag.2006.01.004
22. Sirous H, Zabihollahi R, Aghasadeghi MR, Sadat SM, Saghaie L, Fassihi A. Docking studies of some 5-hydroxypyridine-4-one derivatives: evaluation of integrase and ribonuclease H domain of reverse transcriptase as possible targets for anti-HIV-1 activity. Med Chem Res 2015;24(5):2195-212. doi:10.1007/s00044-014-1289-1
23. Morris GM, Huey R, Lindstrom W, Sanner MF, Belew RK, Goodsell DS, et al. AutoDock4 and AutoDockTools4: automated docking with selective receptor flexibility. J Comput Chem 2009;30(16):2785-91. doi:10.1002/jcc.21256
24. Morris GM, Huey R, Olson AJ. Using AutoDock for ligand-receptor docking. Curr Protoc Bioinformatics 2008; Chapter 8: Unit 8.14. doi:10.1002/0471250953.bi0814s24
25. Heid CA, Stevens J, Livak KJ, Williams PM. Real time quantitative PCR. Genome Res 1996;6(10):986-94. doi:10.1101/gr.6.10.986
26. Rahelivao MP, Lübken T, Gruner M, Kataeva O, Ralambondrahety R, Andriamanantoanina H, et al. Isolation and structure elucidation of natural products of three soft corals and a sponge from the coast of Madagascar. Org Biomol Chem 2017;15(12):2593-608. doi:10.1039/c7ob00191f
27. Kobayashi M, Tomioka A, Mitsuhashi H. Marine sterols. VIII. Isolation and structure of sarcosterol, a new sterol with a Δ17(20)-double bond from the soft coral *Sarcophyton glaucum*. Steroids 1979;34(3):273-93. doi:10.1016/0039-128x(79)90079-5
28. Bowden BF, Coll JC, Dai MC. Studies of Australian soft corals. XLIII. The structure elucidation of a new diterpene from *Alcyonium molle*. Aust J Chem 1989;42(5):665-73. doi:10.1071/ch9890665
29. Pour PM, Yegdaneh A, Aghaei M, Kazemi F, Ghanadian M. Mitochondrial pro-apoptotic properties of *Sinularia compressa* from Persian Gulf against breast cancer cells and its chemical composition. Nutr Cancer 2022;74(6):2276-90. doi:10.1080/01635581.2021.2007961
30. Fernholz E, MacPhillamy HB. Isolation of a new phytosterol: campesterol. J Am Chem Soc 2002;63(4):1155-6. doi:10.1021/ja01849a079
31. Gauvin A, Smadja J, Aknin M, Faure R, Gaydou EM. Isolation of bioactive 5α,8α-epidioxy sterols from the marine sponge *Luffariella* cf. *variabilis*. Can J Chem 2000;78(7):986-92. doi:10.1139/v00-083
32. Meccia G, Rosquete C, Rojas LB, Feliciano AS. New labdane derivative from the essential oil of *Acalypha plicata* Müll. Arg. Flavour Fragr J 2006;21(3):559-61. doi:https://doi.org/10.1002/ffj.1679
33. Stránský K, Zarevúcka M, Valterová I, Wimmer Z. Gas chromatographic retention data of wax esters. J Chromatogr A 2006;1128(1-2):208-19. doi:10.1016/j.chroma.2006.06.035
34. Lipinski CA, Lombardo F, Dominy BW, Feeney PJ. Experimental and computational approaches to estimate solubility and permeability in drug discovery and development settings. Adv Drug Deliv Rev 2001;46(1-3):3-26. doi:10.1016/s0169-409x(00)00129-0
35. Arriaga-Alba M, Montero-Montoya R, Espinosa-Aguirre JJ. The Ames test in twenty-first century. Res Rev J Toxicol 2012;2(1):23-37. doi:10.37591/rrjot.v2i1.1289
36. Wesseling CMJ. Potentiation of Gram-positive specific antibiotics against Gram-negative bacteria through outer membrane disruption. (2022, July 5. Retrieved from https://hdl.handle.net/1887/3421483
37. Koo H, Allan RN, Howlin RP, Stoodley P, Hall-Stoodley L. Targeting microbial biofilms: current and prospective therapeutic strategies. Nat Rev Microbiol 2017;15(12):740-55. doi:10.1038/nrmicro.2017.99
38. Loho T, Sukartini N, Astrawinata DA, Immanuel S, Aulia D, Priatni I. In vitro antibacterial interaction of doripenem and amikacin against multidrug-resistant *Acinetobacter baumannii*, *Pseudomonas aeruginosa*, and *Klebsiella pneumoniae* isolates. Can J Infect Dis Med Microbiol 2018;2018:1047670. doi:10.1155/2018/1047670

39. Roy R, Tiwari M, Donelli G, Tiwari V. Strategies for combating bacterial biofilms: a focus on anti-biofilm agents and their mechanisms of action. Virulence 2018;9(1):522-54. doi:10.1080/21505594.2017.1313372
40. Wang Z, Tang H, Wang P, Gong W, Xue M, Zhang H, et al. Bioactive polyoxygenated steroids from the South China sea soft coral, *Sarcophyton* sp. Mar Drugs 2013;11(3):775-87. doi:10.3390/md11030775
41. Nakashima R, Sakurai K, Yamasaki S, Hayashi K, Nagata C, Hoshino K, et al. Structural basis for the inhibition of bacterial multidrug exporters. Nature 2013;500(7460):102-6. doi:10.1038/nature12300
42. Alav I, Kobylka J, Kuth MS, Pos KM, Picard M, Blair JMA, et al. Structure, assembly, and function of tripartite efflux and type 1 secretion systems in gram-negative bacteria. Chem Rev 2021;121(9):5479-596. doi:10.1021/acs.chemrev.1c00055
43. Verma P, Maurya P, Tiwari M, Tiwari V. In-silico interaction studies suggest RND efflux pump mediates polymyxin resistance in *Acinetobacter baumannii*. J Biomol Struct Dyn 2019;37(1):95-103. doi:10.1080/07391102.2017.1418680
44. Sjuts H, Vargiu AV, Kwasny SM, Nguyen ST, Kim HS, Ding X, et al. Molecular basis for inhibition of AcrB multidrug efflux pump by novel and powerful pyranopyridine derivatives. Proc Natl Acad Sci U S A 2016;113(13):3509-14. doi:10.1073/pnas.1602472113
45. Sarma NS, Krishna MS, Pasha SG, Rao TS, Venkateswarlu Y, Parameswaran PS. Marine metabolites: the sterols of soft coral. Chem Rev 2009;109(6):2803-28. doi:10.1021/cr800503e